nature methods

RESOURCE

https://doi.org/10.1038/s41592-020-0801-4

Meltome atlas—thermal proteome stability across the tree of life

Anna Jarzab[1,10], Nils Kurzawa[2,3,10], Thomas Hopf[4,10], Matthias Moerch[5], Jana Zecha[1], Niels Leijten[6], Yangyang Bian[1], Eva Musiol[7], Melanie Maschberger[4], Gabriele Stoehr[4], Isabelle Becher[2], Charlotte Daly[1], Patroklos Samaras[1], Julia Mergner[1], Britta Spanier[8], Angel Angelov[5], Thilo Werner[9], Marcus Bantscheff[9], Mathias Wilhelm[1], Martin Klingenspor[7], Simone Lemeer[6], Wolfgang Liebl[5], Hannes Hahne[4]✉, Mikhail M. Savitski[2]✉ and Bernhard Kuster[1]✉

We have used a mass spectrometry-based proteomic approach to compile an atlas of the thermal stability of 48,000 proteins across 13 species ranging from archaea to humans and covering melting temperatures of 30–90 °C. Protein sequence, composition and size affect thermal stability in prokaryotes and eukaryotic proteins show a nonlinear relationship between the degree of disordered protein structure and thermal stability. The data indicate that evolutionary conservation of protein complexes is reflected by similar thermal stability of their proteins, and we show examples in which genomic alterations can affect thermal stability. Proteins of the respiratory chain were found to be very stable in many organisms, and human mitochondria showed close to normal respiration at 46 °C. We also noted cell-type-specific effects that can affect protein stability or the efficacy of drugs. This meltome atlas broadly defines the proteome amenable to thermal profiling in biology and drug discovery and can be explored online at http://meltomeatlas.proteomics.wzw.tum.de:5003/ and http://www.proteomicsdb.org.

Proteome-wide analysis of the thermal stability of proteins offers new ways of asking and answering questions in biology and drug discovery[1,2]. For instance, does the thermal proteome stability of organisms coincide with extrinsic stress conditions such as high temperature? If so, to what extent is that related to differences in the intrinsic properties of the proteins (that is, sequence) or the cellular environment? Even within single cells, vital biological processes may take place at different temperatures, as exemplified by a recent report suggesting that mitochondria in human cells operate at close to 50 °C (ref. [3]). This poses the question whether protein thermal stability had to be engineered for such local 'over-heated' environments. One might also ask whether and how mutations affect the stability of proteins in cells, and there are open questions as to why intrinsically disordered proteins can be very thermostable (such as in the case of tau protein) but are overall less thermostable than structured proteins[1]. How functional order can be achieved in a molecularly crowded cell is also an intense area of research, and phase transitions are emerging as an important concept[4,5]. Such phase transitions might be mediated by many factors, including posttranslational modifications or the degree of disordered protein structure, both of which may be measured by thermal proteome profiling (TPP). The literature also shows that TPP has great potential for measuring protein–protein[6–8], protein–metabolite[9,10] and protein–drug interactions[2,11]. Broad empirical information on the thermal stability of proteins may be of substantial interest for protein engineering purposes and biotechnology in general. Even though rapid progress has been made along many of these lines, this emerging field would benefit from the availability of high-quality TPP reference data. Therefore, the authors of this study joined forces to create an atlas of thermal proteome stability across 13 model organisms that can be explored using an online R Shiny App and ProteomicsDB[12,13]. We derive characteristics of protein thermal stability and illustrate the use of the resource on a number of examples addressing several of the aforementioned topics.

Results

Meltome atlas across the tree of life. The atlas (Fig. 1) encompasses 77 data sets from 13 species including six prokaryotes (five bacteria and one archaeon) that live between 4 and 70 °C and seven eukaryotes covering yeast, worm, fish, fly, plant, mouse and human. The atlas contains melting characteristics for ~48,000 nonredundant proteins and the human chapter contains TPP data for 13,000 proteins from 14 cell lines, primary cells, tissues and 5 body fluids (Supplementary Tables 1 and 2). Thermal profiles were generated by heating cells (43 data sets) or lysates (34 data sets), removing the precipitate by centrifugation, digesting the soluble fraction using trypsin, encoding each temperature-specific peptide pool by stable isotopes (tandem mass tags, TMTs), combining samples across all temperatures, separating the peptides by off-line liquid chromatography and subjecting each fraction to online liquid chromatography–tandem mass spectrometry (LC–MS/MS), peptide and protein identification as well as quantification

[1]Chair of Proteomics and Bioanalytics, Technical University of Munich, Freising, Germany. [2]Genome Biology Unit, EMBL, Heidelberg, Germany. [3]Faculty of Biosciences, EMBL and Heidelberg University, Heidelberg, Germany. [4]OmicScouts GmbH, Freising, Germany. [5]Department of Microbiology, Technical University of Munich, Freising, Germany. [6]Biomolecular Mass Spectrometry and Proteomics, Bijvoet Center for Biomolecular Research and Utrecht Institute for Pharmaceutical Sciences, Utrecht University, Utrecht, the Netherlands. [7]Molecular Nutrition Unit, Technical University of Munich, Freising, Germany. [8]Chair of Nutritional Physiology, Technical University of Munich, Freising, Germany. [9]Cellzome, Heidelberg, Germany. [10]These authors contributed equally: Anna Jarzab, Nils Kurzawa, Thomas Hopf. ✉e-mail: hannes.hahne@omicscouts.com; mikhail.savitski@embl.de; kuster@tum.de

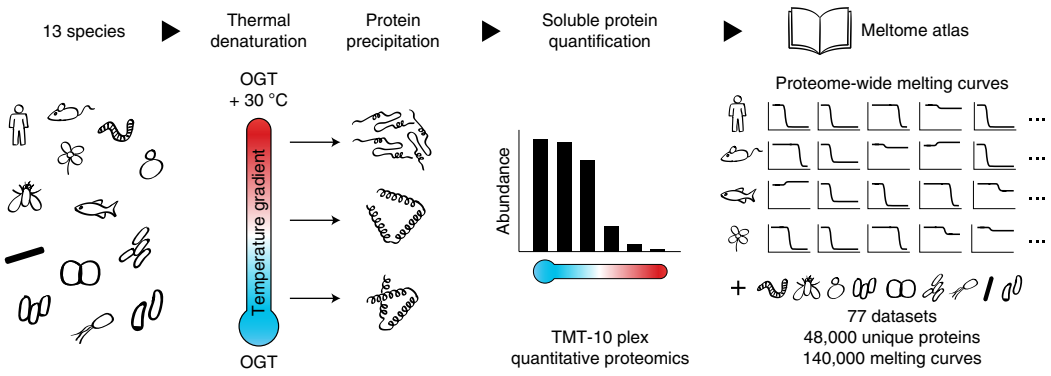

Fig. 1 | Meltome atlas. Schematic representation of the workflow used to compile the melting characteristics of proteins from 13 model organisms.

(Methods). We refer to melting temperatures (T_m, for proteins that show at least 50% precipitation) or area under the (melting) curve (AUC) values (available for all proteins). We note that TPP is not equivalent to temperature-dependent unfolding but the combination of unfolding and precipitation in cells or lysates. Therefore, TPP data may not be directly comparable to data from biophysical methods that measure the thermal stability of isolated proteins (see Seashore-Ludlow et al.[14] for a recent perspective on the challenges of TPP). Examples for thermal profiles of individual proteins are shown in Supplementary Fig. 1. Melting curves of all proteins can be explored in an R Shiny App (http://meltomeatlas.proteomics.wzw.tum.de:5003) or by following hyperlinks in tables deposited in the PRIDE/proteomeXchange repository (data set identifier PXD011929). The TPP data for human proteins are also available in ProteomicsDB[13]. Replicate analysis showed that T_m and AUC measurements were generally well reproducible (Supplementary Fig. 2). An inter-laboratory comparison using human K562 cells also showed that the TPP method is robust as the median of all proteins had T_m and AUC values within 0.5 °C and 3%, respectively, between replicates measured in the same laboratory and no worse than 2.3 °C for T_m and 10% for AUC between laboratories (Supplementary Fig. 2).

The width of the distribution of protein T_m values of the different species ranged from 9 °C in zebrafish (*Danio rerio*) to 20 °C for *Escherichia coli* (90% range; Fig. 2a). All eukaryotes showed a substantial gap between their optimal growth temperature (OGT) and the temperature at which proteins begin to precipitate (that is, the cold side of the T_m distribution). In contrast, for all but one bacterial species, the OGT was close to the cold side of the T_m distribution, and these species do not grow well or at all at even slightly higher temperatures than their OGTs[15]. *Oleispira antarctica* presents a special case. In its natural habitat, the bacterium lives at 2–4 °C, but it can grow between 1 and 25 °C. The peak of its T_m distribution (40 °C) is similar to that of *Caenorhabditis elegans* (OGT of 20 °C). This is noteworthy as it may indicate that most proteins on earth are stable to at least 30 °C. This may be supported by the fact that most enzymes can operate at temperatures much lower than their optima and that even cold-adapted enzymes usually have temperature optima of >20 °C (ref. [10]).

Global gene ontology analysis of the thermally most unstable proteins within or across species did not reveal strong associations to cellular processes or molecular functions. There was also no global association of thermal stability for essential genes as has been suggested before (Supplementary Fig. 3)[1]. Instead, we found that certain particularly unstable proteins serve vital cellular functions, the loss of any of which alone or in combination could lead to cell death. Examples for such proteins that have T_m values as low as 44–46 °C in human A549 lung cancer cell lysate (Supplementary Table 2) include members of the mitochondrial protein synthesis machinery (the translation elongation factor, T_m = 45 °C) and several important metabolic enzymes such as glutaminase (T_m = 44 °C), dihydrofolate reductase (T_m = 44 °C) and methionine aminopeptidase 1 (T_m = 46 °C). We also analyzed the loss of bulk protein by heat-induced precipitation using lysates of human K562 leukemia cells (Supplementary Fig. 4). After just 3 min at 44 °C, ~10% of the total protein had already precipitated, offering a compelling hypothesis for why humans die of hyperthermia-associated multiple organ failure if the core body temperature rises above 42 °C.

For the purpose of the subsequent analysis, we defined four categories of thermal stability. We distinguish proteins with low T_m (AUC < 0.35), medium T_m (AUC 0.35–0.65), high T_m (AUC > 0.65) and nonmelters (no T_m). The proportions of thermally stable or unstable proteins varied between species or cell types (Fig. 2b and Supplementary Fig. 5) with *Drosophila melanogaster* having particularly few nonmelting proteins and *Picrophilus torridus* showing a rather large proportion of thermally unstable proteins. Because *Thermus thermophilus* grows optimally at 70 °C, a larger proportion of its proteins is more heat stable than for most other species. This was also observed for *C. elegans*, the reasons for which are currently unclear. Human body fluids stood out in that they are dominated by nonmelting proteins. We attribute this to their high general solubility, in part due to often extensive glycosylation. We note again that a limitation of TPP is that it cannot measure if a protein thermally denatures but remains soluble.

Factors affecting thermal proteome stability. Some enzymes such as DNA polymerase from *Thermus aquaticus* are very heat stable as purified proteins. This alone demonstrates that amino acid sequence and structure are important determinants of thermal stability. However, it has also been shown that the complex molecular environments of cells play a role[6]. To extend previous investigations, we compared the thermal profiles of proteins in cells versus lysates using *E. coli* (OGT 37 °C) and *T. thermophilus* (OGT 70 °C) as examples (Fig. 3a). The median T_m values of proteins from both species are >30 °C apart, and many proteins show differences between cells and lysates. Reasons for the latter may include the loss of membranes during lysis; the disruption of protein complexes; the presence of osmoprotectants; and the dilution of proteins, cofactors or solutes, to name a few. We then prepared separate lysates from the two species and mixed them in equal quantities before heating (Fig. 3b). The median T_m values for both species were nearly identical to the ones obtained from the separate lysate experiments (Spearman's r = 0.75 for *E. coli* and r = 0.83 for *T. thermophilus*), showing that the mere presence of proteins from one species did not substantially influence the melting behavior of proteins from the other. The lysate data were much more tightly correlated (Fig. 3b) than the cell versus lysate experiment (Fig. 3a), indicating that the cellular context does have an effect on protein stability. In a third

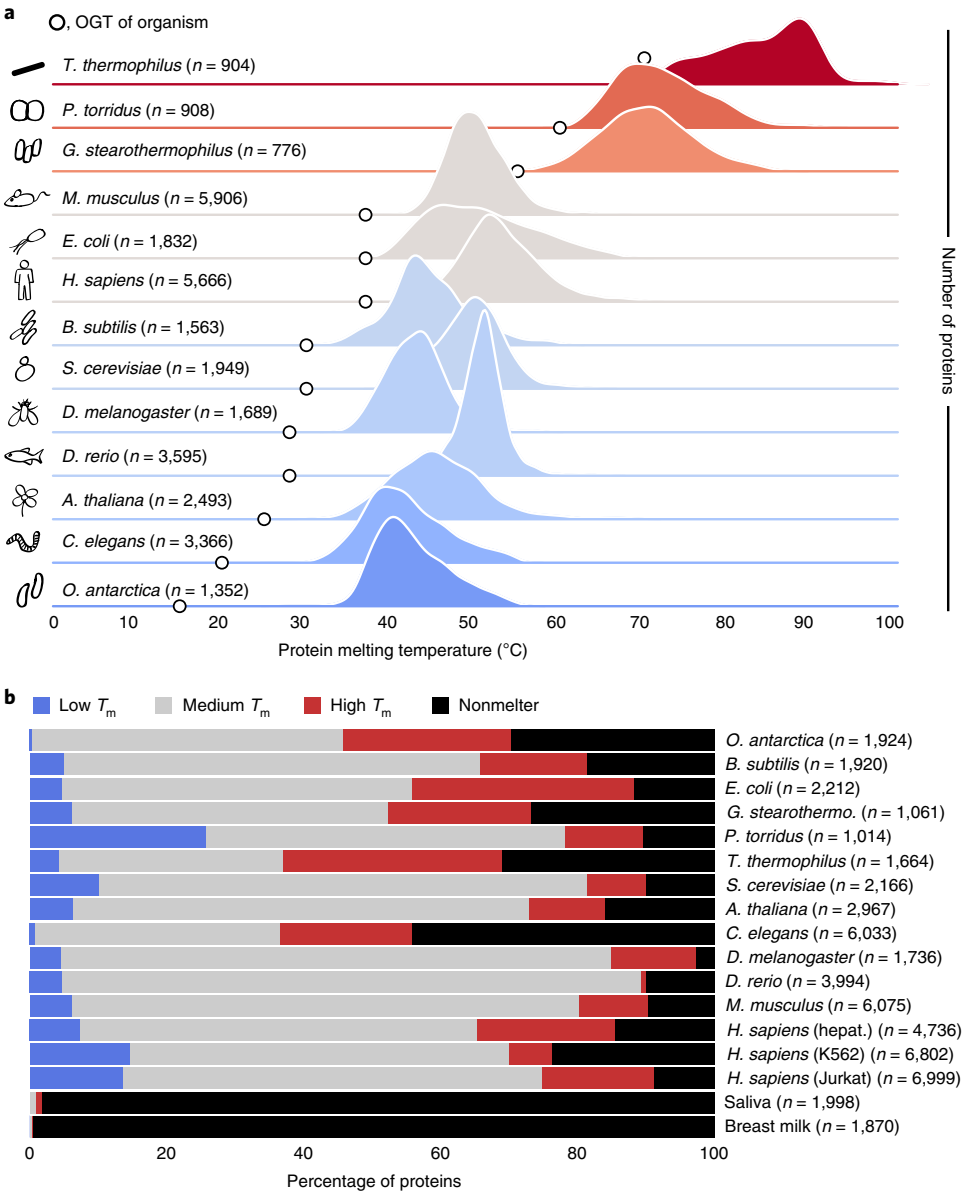

Fig. 2 | Meltome atlas across the tree of life. a, Distribution of T_m of proteins of the 13 organisms investigated in this study ordered by their OGT (marked by open circles, data from lysates experiments shown). **b**, Distribution of the melting characteristics (lysates) of each species classified into proteins with low, medium, high and no melting point. Numbers in parentheses denote the number of proteins quantified in each sample.

experiment, we expressed a subset of *T. thermophilus* proteins in *E. coli* cells and observed again that the T_m values of proteins from both species were largely unaffected (Fig. 3c). Together, this shows that protein sequence/structure is one dominant determinant of absolute thermal protein stability but that the cellular environment has a substantial influence too. Indeed, by comparing TPP experiments on human cells and lysates in parallel, it has been shown that proteins can show differences depending on cellular localization[11]. The many TPP experiments assembled here substantially expanded the scope of such analysis. For example, TPP data for intracellular proteins identified in human body fluids (as the result of cell shedding from, for example, blood vessels or glandular ducts; see Fig. 3d) showed that protein concentration also plays a role. For the 25 cases shown, it is apparent that these proteins are generally more soluble in body fluids than in cells on heating (that is, have substantially higher AUC values). It therefore appears that these proteins are unable to aggregate because their individual protein concentrations are very low. They can also not coaggregate with other proteins despite high overall protein concentration in the body fluids because the latter proteins generally do not precipitate on heat treatment. A further possibility is the presence of aggregation-suppressing emulsifiers such as lecithins in human milk[16]. We found many examples of coaggregating proteins that are part of protein complexes[2,8]. Upon comparison of the TPP behavior of the Arp2/3 complex in zebrafish and human (Fig. 3e and Supplementary Fig. 6 for the CCR-NOT complex), it appears that protein complexes are conserved in how tightly they are assembled even though their absolute T_m values are substantially different. We analyzed this more systematically for *Homo sapiens*, *Mus musculus*, *D. rerio*, the EcoCyc database, *E. coli*, yeast and *D. melanogaster*[17–20], which confirmed that codenaturation of protein complex subunits is often conserved even across distantly related species. As observed by Tan et al. for human cells[8] and Mateus et al. for *E. coli*[11], this approach recovered more complexes for experiments performed with intact cells than with lysates (Supplementary Fig. 6).

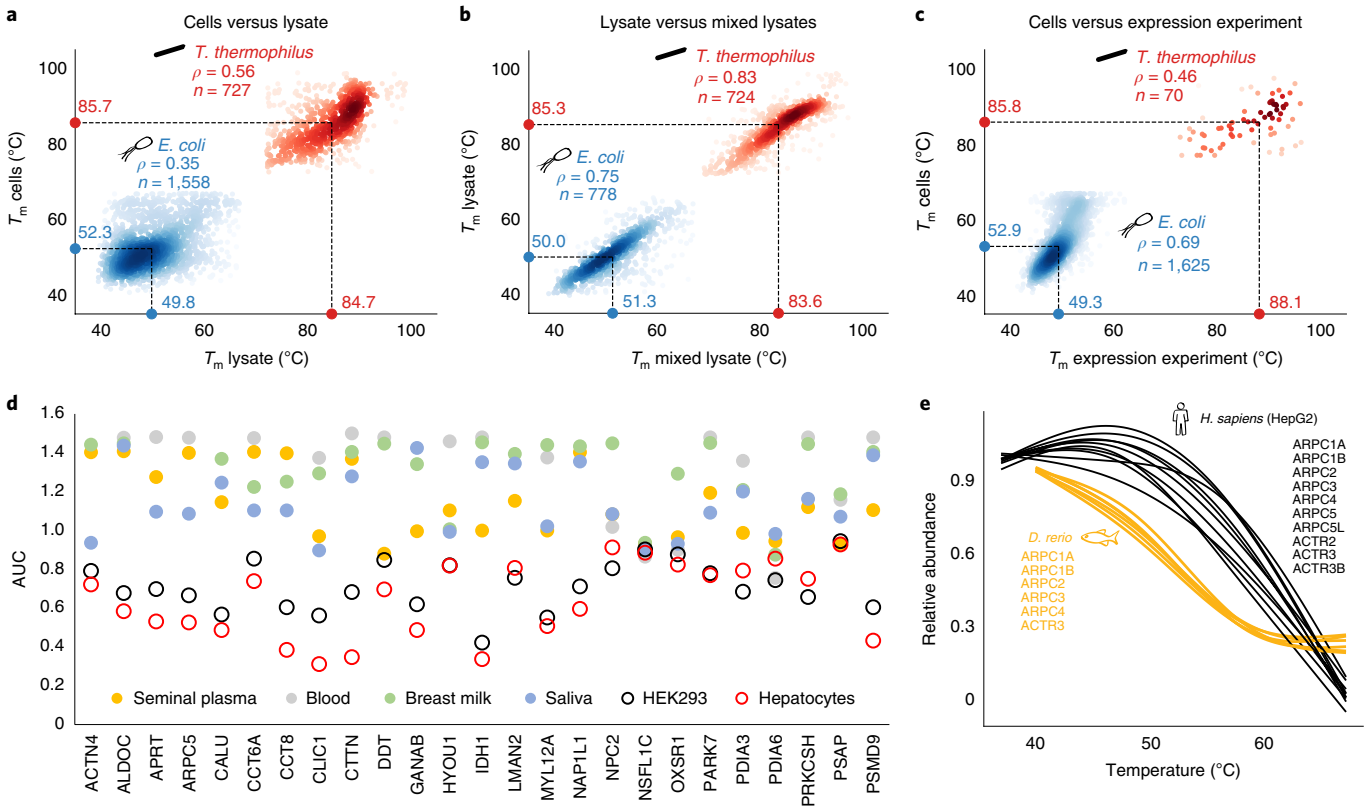

Fig. 3 | Global determinants of thermal protein stability. a, Comparison of the melting points of proteins from *E. coli* and *T. thermophilus* obtained from heating intact cells or lysates thereof in separate experiments. The median melting point for each species and experiment is indicated by dashed lines and colored circles, and the correlation of melting points within a species is given by Spearman correlation coefficients. **b**, Same as **a** but when mixing equal quantities of lysates before heating. **c**, Same as **a** but when expressing *T. thermophilus* proteins in *E. coli* followed by heating of cells. **d**, Analysis of the thermal stability of 25 intracellular human proteins (expressed as AUC) detected in seminal plasma, blood, breast milk, saliva, HEK293 cells and primary hepatocytes. **e**, Comelting behavior of members of the Arp2/3 complex in *D. rerio* ($n=1$) and human HepG2 cells ($n=3$).

As reported before[1,11], there was a statistically highly significant negative association between the length of proteins and their thermal stability (Fig. 4a). We found this association consistently in almost all data sets but point out that the correlations are generally weak and the effect sizes are very small (Supplementary Fig. 7). Therefore, for proteins within one species, the association of T_m and length has little predictive value. In contrast, correlating the mean protein length with the mean T_m values across bacterial species showed a clearer association (Pearson $r=-0.59$, $P=0.22$) and a larger effect (slope of −1.04, Fig. 4b). Albeit not statistically strong, this is interesting because producing larger proteins is one of the few ways for bacteria to generate proteins with advanced structures, but the data across species indicate that life at higher temperatures comes at the cost of the need to restrict protein size. In line with this, increased compactness and the truncation of solvent-exposed loops are among the factors that may render proteins extremely thermostable[21]. We found no such association for the eukaryotic species, all of which live at ambient temperature (Fig. 4b). For *E. coli*, Leuenberger et al.[1] had shown that protein abundance correlated with thermal stability. We observed the same overall trend in most of our data sets, and the effect was more pronounced in nonmelting proteins, a group that the Leuenberger study did not consider (Fig. 4c, mouse bone marrow derived cells, see Supplementary Fig. 8). But again, the correlations are very weak (average Pearson $r=0.16$ for T_m and $r=0.17$ for AUC) and the effect sizes are very small (average slope of 0.74 for T_m and 0.03 for AUC), so that protein abundance cannot be considered a good predictor of thermal stability.

We next considered amino acid composition and found that *T. thermophilus* proteins have a substantially lower cysteine content than other species. For most other amino acids, no clear associations were observed. However, when grouped by certain properties, we found that proteins of the thermophile *T. thermophilus* contained far fewer polar amino acids than those of the mesophile *E. coli* (Fig. 4d), corroborated by a similar observation for *Geobacillus stearothermophilus* versus *Bacillus subtilis* (Supplementary Figs. 9 and 10). Conversely, *T. thermophilus* proteins had a slightly higher frequency of hydrophobic amino acids (Fig. 4e), in line with the previous observation that, for example, increasing hydrophobic interactions in the core leads to more stable structures[22–25]. Even though there were clear differences in the frequency of helical, loop or strand structures between bacteria and eukaryotes, their relative proportions were nearly identical between bacteria even though their OGTs differed by >50 °C (Fig. 4f). Notably, loops and disordered regions are far more prevalent in the proteins of eukaryotic species than in prokaryotes (Fig. 4g). We therefore assessed whether the extent of disordered regions in human proteins may be a predictor of thermal stability in situ. Previous work using lysates has shown that proteins with large proportions of disordered regions are often thermally unstable and exhibit similar melting behavior as structured proteins[1]. Our TPP data for human proteins corroborated this observation for whole cells (Supplementary Fig. 11), and our AUC stability classification allowed us to extend this analysis to nonmelting proteins. Against this trend, nonmelters were most strongly enriched in disordered regions (Fig. 4h). Nonmelting proteins exhibited a bimodal distribution in terms of disordered

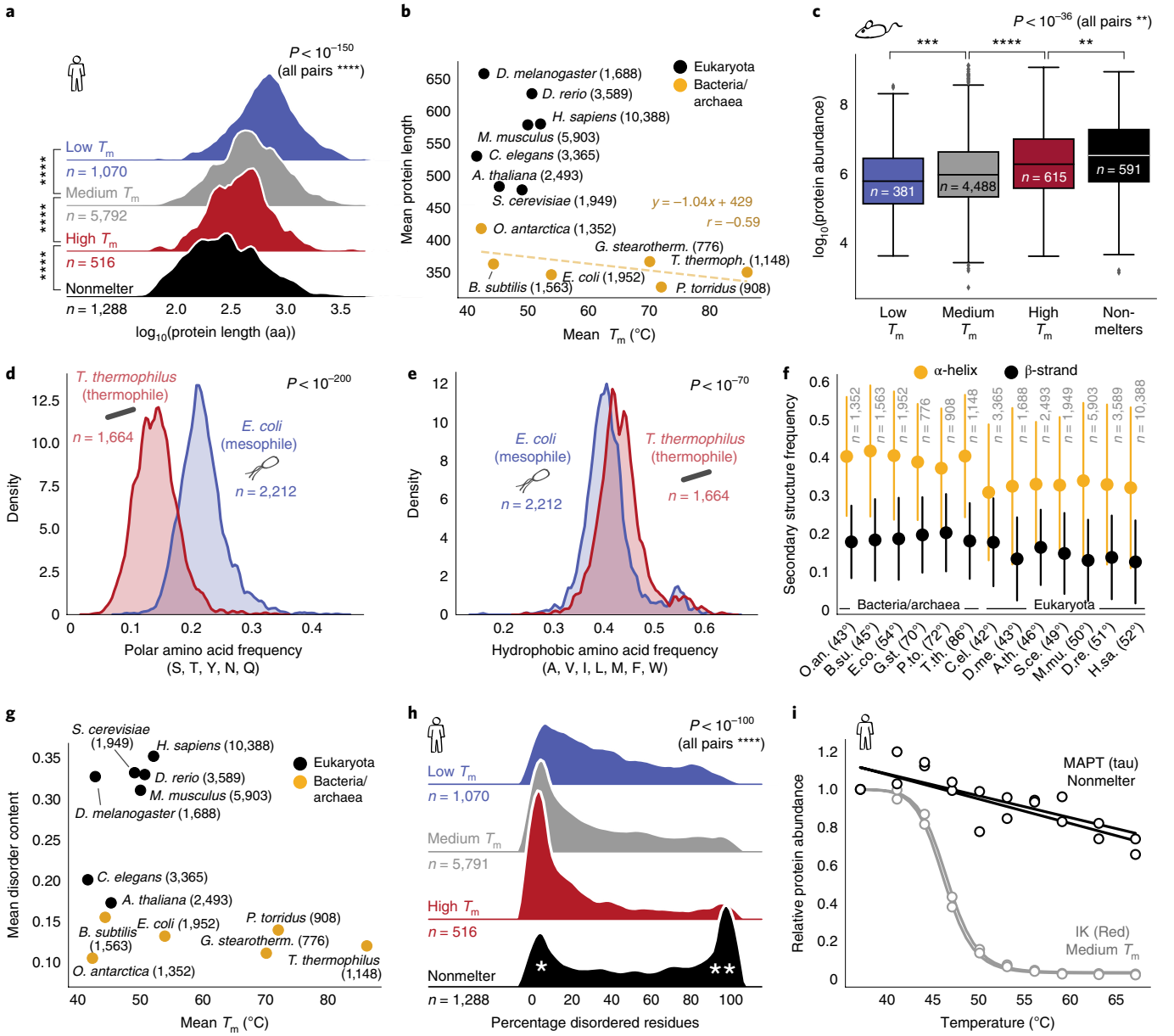

Fig. 4 | Molecular determinants of thermal protein stability (lysate data). a, Analysis of the association of protein length and T_m within a species using *E. coli* as an example. Thermally stable proteins tend to be smaller than heat-labile proteins. Asterisks mark statistically significant differences between the melting categories (Kruskal–Wallis test with Dunn's post hoc test, multiple testing correction according to Benjamini–Hochberg; ****$P < 0.0001$). **b**, Similar to **a** but across species. Circles mark the mean T_m of all proteins in a species. The dotted line represents the linear regression analysis of mean T_m values across prokaryotes, revealing a rather strong association that is not observed for eukaryotes (r, Pearson's correlation coefficient; number of data points per species in parentheses). **c**, Analysis of the association of protein abundance and T_m of murine bone marrow-derived cells as an example (Kruskal–Wallis test with Dunn's post hoc test, multiple testing correction according to Benjamini–Hochberg; **$P < 0.01$, ***$P < 0.001$, ****$P < 0.0001$; box plot, box corresponds to quartiles of the distribution, whiskers extend to the first data point inside the first/third quartile plus 1.5 × interquartile range (IQR), respectively). **d**, Distribution of the frequency of polar amino acids in *T. thermophilus* and *E. coli* (P value according to two-sided Mann–Whitney U-test). **e**, Same as **d** but for hydrophobic amino acids. **f**, Frequency of secondary structure elements in all species. Circles denote mean values for all proteins and error bars represent standard deviation. Species names on the x axis are abbreviated and mean T_m values for their proteins are given (sample sizes apply to both secondary structure types). **g**, Mean content of disordered structure elements of proteins as a function of the mean T_m of proteins in each species (number of data points per species in parentheses). **h**, Distribution of disordered structure content of human proteins in the four melting categories used in this study. An asterisk marks proteins enriched in extracellular proteins and a double asterisk denotes enrichment in nuclear and phosphorylated proteins (statistical test and significance markers as in **a**). **i**, Melting curves ($n = 2$) for two highly disordered proteins either exhibiting medium (IK, protein Red) or high (tau) thermal stability in U937 cells.

structure. Gene ontology analysis revealed that nonmelters with little disordered structure were strongly enriched in transmembrane-domain-containing proteins, proteins with extracellular domains, glycosylated proteins, secreted proteins with signal peptides and proteins containing disulfide bonds, all of which provide a rationale for why these proteins do not precipitate at higher temperatures. In contrast, heat-stable but highly unstructured proteins were strongly enriched in nuclear proteins and proteins

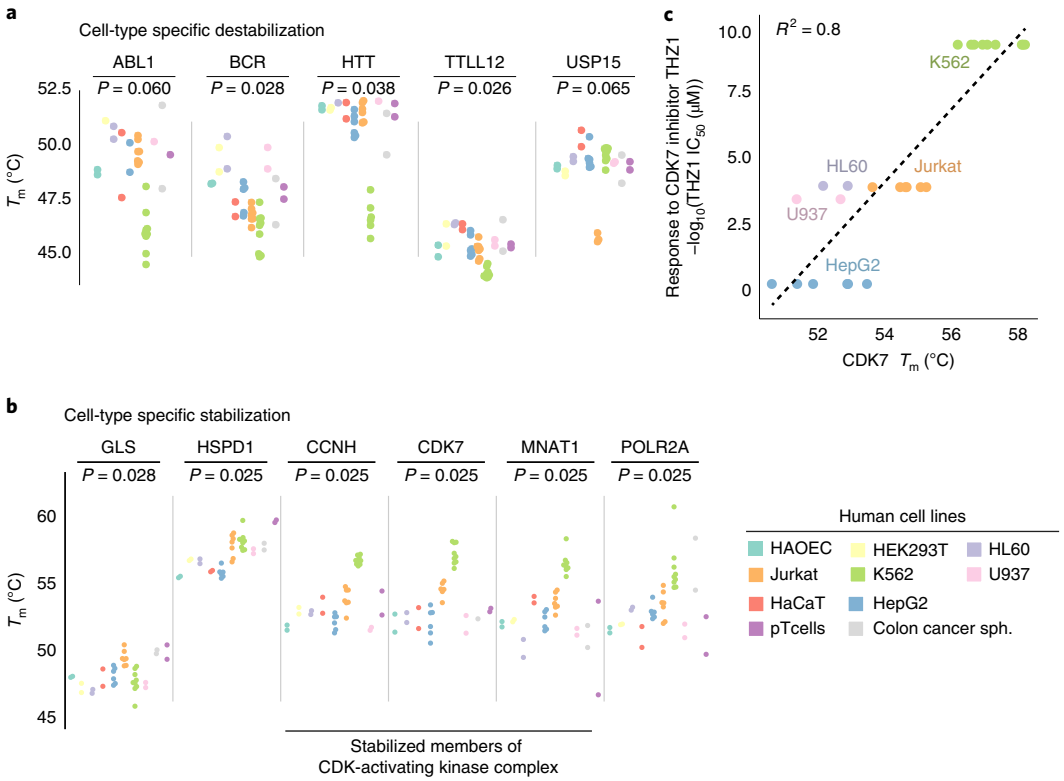

Fig. 5 | Human meltome atlas. a, T_m values of five example proteins with genetic lesions that are cell-type-specifically destabilized in certain cell types. **b**, Same as **a** but for proteins that are cell-type-specifically stabilized in certain cell types. The Kruskal–Wallis and Dunn's post hoc tests were used to assess statistical significance in **a** and **b**. **c**, Correlation analysis of the T_m values of CDK7 and IC_{50} values of the antiproliferative activity of the covalent CDK7 inhibitor THZ1 in different cell types ($n \geq 2$ biologically independent experiments) (THZ1 antiproliferative activity data taken from Kwiatkowski et al.[34]; R^2 denotes the squared Pearson correlation coefficient).

annotated to be phosphorylated (Supplementary Table 3). The group of highly disordered proteins contained tau, which is almost entirely disordered and well known to be heat resistant (Fig. 4i)[26]. In contrast, the spliceosomal protein IK (protein Red, both from U937 cells) is also a largely disordered protein but showed a T_m of about 47 °C. We can conclude that there is a more complex relationship between disorder and thermal protein stability than previously appreciated.

Our experiments suggest that protein stability is, in large parts, an intrinsic property of proteins encoded in their primary sequence. But is this property conserved evolutionarily between different species; that is, do proteins maintain their stability as they evolve? To test this hypothesis, we compared relative protein stabilities across all 13 species by computing correlations between the AUCs of orthologous proteins (Methods). Hierarchical clustering of the correlation coefficients (Supplementary Fig. 12) approximately recovered the known phylogenetic relationship between the analyzed species, with two broad clusters for bacteria/archaea and eukaryotes. The eukaryotic subcluster mostly followed the species tree of eukaryotes from yeast to mammals, with the highest correlation observed between mouse and human ($r = 0.62$), as would be expected by the relatively small evolutionary distance between the two species. These findings suggest that protein stability is at least partly a conserved property but continually decreases as the sequences (and the environmental pressures shaping them) diverge.

Meltome atlas of human cell types. The human meltome data sets comprise three primary cell types, colon cancer spheroids and ten commonly used cell lines (Supplementary Table 1). To identify potential cell-type-specific differences, we compared proteins for which melting points were determined across all cell types. We observed clustering of replicates and an overall concordant melting behavior (Supplementary Fig. 5c). Next, we devised a strategy to identify proteins with specifically higher or lower melting points in individual cell types. We tested 7,278 proteins for which T_m could be estimated in at least three different cell types (Methods) and observed clusters of proteins that show a cell-type-specific melting characteristic (Supplementary Fig. 5d). We found that many (statistically significantly) cell-type-specifically destabilized proteins had altered genotypes (Fig. 5a). It is not clear to what extent this may be generalized, but, in line with previous results, we observed lower thermal stability of the proteins BCR and ABL1 in K562 cells, which are functionally characterized by the fusion of the two genes. The fusion protein is also highly unstable in primary cells from patients with chronic myelogenous leukemia[27]. We also found the protein underlying Huntington's disease (huntingtin, HTT) to be both very unstable and decreased in abundance in these cells compared to all other cell types[28]. HTT was recently found to harbor a disruptive in-frame insertion in K562 cells[29], and one might speculate if this alteration may explain its decreased stability and abundance. Similarly, we found ubiquitin carboxyl-terminal hydrolase 15 (USP15) to be specifically and strongly destabilized in Jurkat cells in which it was found to harbor multiple single nucleotide variants and deletions[30]. Tubulin-tyrosine ligase-like protein 12 (TTLL12) was found to be mildly destabilized in K562 cells and is reported to harbor a missense single nucleotide variant in this cell line[29]. While we and others have reported that thermal stability is not generally associated with protein degradation rates[1,6,31], these observations provide some basis to speculate that even small changes to a

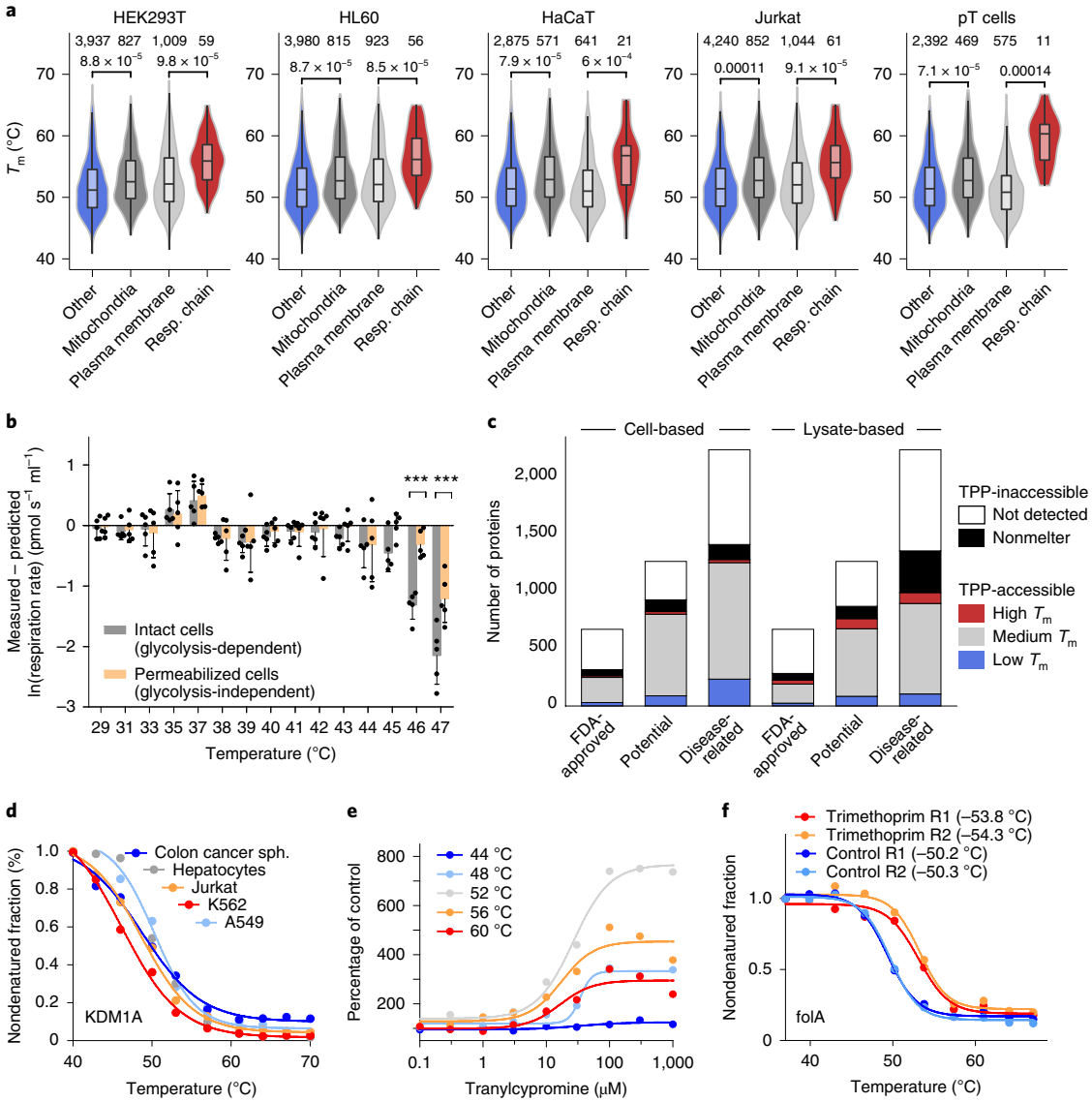

Fig. 6 | Heat stability of proteins of the mitochondrial respiratory chain and use of the meltome atlas in drug discovery. a, Distribution of melting points of mitochondrial, plasma membrane and respiratory chain proteins compared to other proteins (cell-based TPP). Numbers above the violin plots denote the number of proteins in each category and the numbers below denote the statistical significance of the observed differences (bootstrap *P* values obtained for testing against the null hypothesis that the difference of the means is zero, confidence level of 0.95). Statistical significance was assessed using a two-sided bootstrap independent two-samples test. The center line in box plots represents the median, the bounds of the boxes indicate the 75 and 25% percentiles—that is, the interquartile range (IQR)—and whiskers correspond to the highest or lowest respective value or, if the lowest or highest value is an outlier (greater than 1.5 × IQR from the bounds of the boxes), to 1.5 × IQR. **b**, Differences in respiration rates of intact and permeabilized HEK293 cells. Permeabilized cells show close to normal respiration at 46 °C while respiration is significantly reduced at these temperatures in intact cells (Bonferroni-corrected *P* values obtained by two-factor (temperature × intact/permeabilized) ANOVA, ***$P < 0.001$). Each box plot represents the mean of $n = 5$ experiments and whiskers indicate the s.d. **c**, Distribution of annotated drug targets, potential drug targets and disease-related proteins in the meltome atlas by thermal stability class in cells or lysates. **d**, Melting curves for the drug-target KDM1A in different human cell types. **e**, Two-dimensional TPP profile of the drug tranylcypromine and its target protein KDM1A in human THP1 cells. **f**, Thermal shift assay in *E. coli* for the antibiotic drug trimethoprim (versus DMSO control) and its protein target folA (data from two replicates shown).

particular protein sequence (and structure) can destabilize a protein and that accumulation of such events or larger genetic lesions may have detrimental effects on protein thermal stability.

Conversely, for (statistically significant) cell-type-specifically stabilized proteins, we observed that they typically participate in cellular processes that are highly active in these cell types (Fig. 5b). For example, glutaminase was specifically stabilized in Jurkat and primary T cells. This enzyme is activated by ADP (potentially stabilized by binding ADP) and converts glutamine to glutamate. This might reflect an enhanced metabolism of glutamine within T lymphocytes that is required for, as an example, glutathione synthesis[32]. Along the same lines, we observed that proteins of the glycolysis pathway (but not the citric acid cycle) were more stable than other proteins in cancer cell lines but not in primary cells (Supplementary Fig. 13), possibly reflecting a stabilizing effect by the bound glycolytic metabolites. The mitochondrial heat shock protein HSPD1 was more stable in colon cancer spheroids than in other cell types, and one might hypothesize that a high HSP cargo load may stabilize the protein. This is consistent with reports showing that chaperones become more thermostable when active[11].

The observation in colon cancer spheroids also agrees with the general finding that high chaperone activity in, for example, colon cancer is associated with poor colorectal cancer prognosis[33].

We observed that all members of the CDK activating kinase (CAK) complex (CDK7, CCNH, MNAT1) coaggregated and exhibited higher thermal stability in K562 cells and, to a lesser extent, in Jurkat cells (Fig. 5b). The activity of this complex is regulated by phosphorylation and has been linked to transcriptional addiction in T cell acute lymphoblastic leukemia[34]. One might speculate that the higher thermal stability of the complex is a consequence of higher activity and thus reflects a stronger dependence of cells on its activity to drive transcription of genes they are addicted to (for example, MYC or RUNX1). In line with this hypothesis, we observed that the large subunit of RNA polymerase II (POL2RA) exhibited a similar pattern of melting points across cell types as the CAK complex (Fig. 5b), and it has previously been shown that POLR2A activity is correlated with thermal stability[6]. Since the catalytic activity of the complex is implemented by the CDK7, we hypothesized that cells with higher thermal stability of the CAK complex would show increased sensitivity to CDK7 inhibitors. Indeed, melting points of CDK7 collected in this study and reported IC_{50} values of antiproliferative activity of the covalent CDK7 inhibitor THZ1 in different cell types[34] correlated well ($R^2 = 0.8$, Fig. 5c) indicating that the drug may also be effective in other leukemias such as chronic or acute myeloid leukemia. Although not investigated here, this indicates that extending TPP to post-translational protein modifications such as phosphorylation, acetylation or glycosylation beyond individual proteins[35] may be a promising future line of research.

Thermal protein stability in the mitochondrial respiratory chain. It has been suggested that mitochondria in human cells are physiologically maintained at close to 50 °C and that some resident enzymes, notably in complexes II, III and IV, have maximal activity between 46–50 °C (ref. [3]). This may not be surprising as a substantial amount of energy is heat dissipated at the site of respiration in mitochondria as a result of proton leakage. However, this implies that steep thermal gradients must exist on the subcellular level, preventing thermal damage to the overall mitochondrial and cellular proteome, and that the proteins exposed to the heat must be sufficiently stable. And indeed, while mitochondrial proteins were not substantially more stable than others, members of the respiratory chain showed robustly higher T_m values, particularly in primary T cells (median T_m of 60 °C; Fig. 6a and Supplementary Fig. 14). To follow up, we measured respiration rates of intact and permeabilized human embryonic kidney 293 (HEK293) cells at different temperatures (Methods). The respiration rate of intact cells, relying on functional upstream glycolytic enzymes, rapidly declined at temperatures above 42 °C. In contrast, permeabilized cells that were externally supplied with substrates for the respiratory chain had close to normal respiration rates at 46 °C (Fig. 6b, Supplementary Table 4 and Supplementary Fig. 15), supporting the hypothesis that proteins of the respiratory chain may have evolutionarily adapted to higher local temperatures by increasing their thermal stability.

Meltome atlas and drug discovery. TPP has proved valuable for target identification and measuring drug–target engagement in cells[2,36]. One contribution of the current study to this field is that it broadly defines the proteins that are amenable to TPP drug profiling experiment today (Fig. 6c and Supplementary Fig. 16). Of the 671 annotated human drug targets, 1,265 potential drug targets and 2,242 disease-related proteins[37,38], 318 (929, 1,413) were detected in cell-based TPP experiments (285/872/1,357 in lysate-based experiments). For 56, 103 and 132 of these, respectively, no T_m could be determined (59/108/365 for lysates), confining these proteins to an AUC analysis or making a TPP drug assay difficult. The remaining 264 (826/1,281) proteins in cells and 226/764/992 in lysates are, in principle, amenable to TPP, but there is as of today no way of predicting which proteins would show a drug-induced stabilization or destabilization effect and how strong the effect might be. As improvements are made to the technology—for example, intact membrane protein extraction procedures—the number of proteins amenable to TPP profiling may continue to rise in the future. The fact that our atlas provides melting characteristics of a large number of proteins can help to configure drug–target engagement assays for selected proteins that may be read out by western blotting or mass spectrometry.

As an example, we examined the interaction of the lysine-specific histone demethylase 1A (KDM1A) with tranylcypromine. The primary use of the drug is to treat depression by way of inhibiting monoamine oxidases A and B. The molecule also inhibits KDM1A by covalently binding to FAD, a cofactor of KDM1A, and is currently in clinical trials as a combination therapy with all-*trans* retinoic acid for the treatment of acute myeloid leukemia (www.clinicaltrials.gov). TPP analysis in several human cell types revealed T_m values between 48 °C in K562 cells and 52 °C in hepatocytes (Fig. 6d). We next performed two-dimensional TPP experiments (that is, varying temperature and drug dose[39]) in THP1 cells (Fig. 6e). It is apparent that the choice of temperature is a compromise: if the temperature is too low (here 44 °C), it is difficult to measure a stabilizing effect because the protein has not yet melted. If the temperature is too high (here 60 °C), measuring the interaction is also compromised because almost all of the protein has already precipitated. Dose-dependent TPP experiments are ideally performed at a temperature higher than the T_m of the protein to maximize the measurable effect (here 52 °C). As a second example, we investigated targets of the antibiotic trimethoprim in *E. coli*. (Fig. 6f and Supplementary Fig. 17). The difference of ~4 °C between the melting curves of the protein FolA (dihydrofolate reductase) in the presence or absence of trimethoprim identified FolA as a target. We note that it is generally required to perform drug-centric TPP experiments in replicates to be able to interpret such rather subtle shifts in T_m values. Again, the value of the data assembled in the meltome atlas is that it provides guidance for selecting an appropriate temperature range for a TPP experiment for a particular protein.

Discussion

We have accumulated melting characteristics of tens of thousands of proteins across 13 organisms from different parts of the tree of life. The scope of the study has enabled an in-depth investigation of the relationships between protein stability, protein sequence, protein function and protein–protein interactions. Mining the atlas revealed that protein thermal stability not only correlates with the OGTs at which different species thrive, but also reflects particular physiological and pathological molecular contexts. The analysis uncovered new factors governing protein thermal stability and showed that disordered proteins fall into two distinct classes. For human cell lines, we observed that differences in thermal stability reflected the difference in activity of biological processes. We also showed that some proteins of the respiratory chain are consistently more thermally stable, in line with locally higher temperatures. We anticipate TPP will continue to be useful in drug discovery, notably for small molecule target deconvolution and target engagement measurements, and we demonstrated that the data can be used to set up such experiments efficiently. The TPP data reported here will likely motivate others to extend investigations in the context of drug discovery, protein engineering and basic biology research. To foster such further use, all data are available via the proteomeXchange consortium and can be explored online using an R Shiny App and ProteomicsDB[13,40].

Online content

Any methods, additional references, Nature Research reporting summaries, source data, extended data, supplementary information,

acknowledgements, peer review information; details of author contributions and competing interests; and statements of data and code availability are available at https://doi.org/10.1038/s41592-020-0801-4.

Received: 2 July 2019; Accepted: 12 March 2020;
Published online: 13 April 2020

References

1. Leuenberger, P. et al. Cell-wide analysis of protein thermal unfolding reveals determinants of thermostability. *Science.* **355**, eaai7825 (2017).
2. Savitski, M. M. et al. Tracking cancer drugs in living cells by thermal profiling of the proteome. *Science* **346**, 1255784 (2014).
3. Chretien, D. et al. Mitochondria are physiologically maintained at close to 50 degrees C. *PLoS Biol.* **16**, e2003992 (2018).
4. Rai, A. K., Chen, J. X., Selbach, M. & Pelkmans, L. Kinase-controlled phase transition of membraneless organelles in mitosis. *Nature* **559**, 211–216 (2018).
5. Patel, A. et al. A liquid-to-solid phase transition of the ALS protein FUS accelerated by disease mutation. *Cell* **162**, 1066–1077 (2015).
6. Becher, I. et al. Pervasive protein thermal stability variation during the cell cycle. *Cell* **173**, 1495–1507 e1418 (2018).
7. Dai, L. et al. Modulation of protein-interaction states through the cell cycle. *Cell* **173**, 1481–1494 e1413 (2018).
8. Tan, C. S. H. et al. Thermal proximity coaggregation for system-wide profiling of protein complex dynamics in cells. *Science* **359**, 1170–1177 (2018).
9. Reinhard, F. B. et al. Thermal proteome profiling monitors ligand interactions with cellular membrane proteins. *Nat. Methods* **12**, 1129–1131 (2015).
10. Siddiqui, K. S. & Cavicchioli, R. Cold-adapted enzymes. *Annu. Rev. Biochem.* **75**, 403–433 (2006).
11. Mateus, A. et al. Thermal proteome profiling in bacteria: probing protein state in vivo. *Mol. Syst. Biol.* **14**, e8242 (2018).
12. Samaras, P. et al. ProteomicsDB: a multi-omics and multi-organism resource for life science research. *Nucleic Acids Res.* **48** (D1), D1153–D1163 (2019).
13. Schmidt, T. et al. ProteomicsDB. *Nucleic Acids Res.* **46**, 1271–1281 (2018).
14. Seashore-Ludlow, B., Axelsson, H. & Lundback, T. Perspective on CETSA Literature: toward more quantitative data interpretation. *SLAS Disco.* **25**, 118–126 (2019). 2472555219884524.
15. Van Derlinden, E. & Van Impe, J. F. Modeling growth rates as a function of temperature: model performance evaluation with focus on the suboptimal temperature range. *Int. J. Food Microbiol.* **158**, 73–78 (2012).
16. Le, T. T. et al. Hydrophilic lecithins protect milk proteins against heat-induced aggregation. *Colloids Surf. B.* **60**, 167–173 (2007).
17. Guruharsha, K. G. et al. A protein complex network of *Drosophila melanogaster*. *Cell* **147**, 690–703 (2011).
18. Keseler, I. M. et al. The EcoCyc database: reflecting new knowledge about *Escherichia coli* K-12. *Nucleic Acids Res.* **45**, 543–550 (2017).
19. Mukhopadhyay, A., Ray, S. & De, M. Detecting protein complexes in a PPI network: a gene ontology based multi-objective evolutionary approach. *Mol. Biosyst.* **8**, 3036–3048 (2012).
20. Ori, A. et al. Spatiotemporal variation of mammalian protein complex stoichiometries. *Genome Biol.* **17**, 47 (2016).
21. Sterner, R. & Liebl, W. Thermophilic adaptation of proteins. *Crit. Rev. Biochem. Mol. Biol.* **36**, 39–106 (2001).
22. Jaenicke, R. & Bohm, G. The stability of proteins in extreme environments. *Curr. Opin. Struct. Biol.* **8**, 738–748 (1998).
23. Nick Pace, C., Scholtz, J. M. & Grimsley, G. R. Forces stabilizing proteins. *FEBS Lett.* **588**, 2177–2184 (2014).
24. Zeldovich, K. B., Berezovsky, I. N. & Shakhnovich, E. I. Protein and DNA sequence determinants of thermophilic adaptation. *PLoS Comput. Biol.* **3**, e5 (2007).
25. Zhou, X. X., Wang, Y. B., Pan, Y. J. & Li, W. F. Differences in amino acids composition and coupling patterns between mesophilic and thermophilic proteins. *Amino Acids* **34**, 25–33 (2008).
26. Weingarten, M. D., Lockwood, A. H., Hwo, S. Y. & Kirschner, M. W. A protein factor essential for microtubule assembly. *Proc. Natl Acad. Sci. USA* **72**, 1858–1862 (1975).
27. Weerkamp, F. et al. Flow cytometric immunobead assay for the detection of BCR-ABL fusion proteins in leukemia patients. *Leukemia* **23**, 1106–1117 (2009).
28. Geiger, T., Wehner, A., Schaab, C., Cox, J. & Mann, M. Comparative proteomic analysis of eleven common cell lines reveals ubiquitous but varying expression of most proteins. *Mol. Cell Proteom.* **11**, M111 014050 (2012).
29. Zhou, B. et al. Comprehensive, integrated, and phased whole-genome analysis of the primary ENCODE cell line K562. *Genome Res.* **29**, 472–484 (2019).
30. Gioia, L., Siddique, A., Head, S. R., Salomon, D. R. & Su, A. I. A genome-wide survey of mutations in the Jurkat cell line. *BMC Genomics* **19**, 334 (2018).
31. Zecha, J. et al. Peptide level turnover measurements enable the study of proteoform dynamics. *Mol. Cell Proteom.* **17**, 974–992 (2018).
32. Chang, W. K., Yang, K. D., Chuang, H., Jan, J. T. & Shaio, M. F. Glutamine protects activated human T cells from apoptosis by up-regulating glutathione and Bcl-2 levels. *Clin. Immunol.* **104**, 151–160 (2002).
33. Dundas, S. R., Lawrie, L. C., Rooney, P. H. & Murray, G. I. Mortalin is over-expressed by colorectal adenocarcinomas and correlates with poor survival. *J. Pathol.* **205**, 74–81 (2005).
34. Kwiatkowski, N. et al. Targeting transcription regulation in cancer with a covalent CDK7 inhibitor. *Nature* **511**, 616–620 (2014).
35. Liu, H. et al. Impact of IgG Fc-oligosaccharides on recombinant monoclonal antibody structure, stability, safety, and efficacy. *Biotechnol. Prog.* **33**, 1173–1181 (2017).
36. Martinez Molina, D. et al. Monitoring drug target engagement in cells and tissues using the cellular thermal shift assay. *Science* **341**, 84–87 (2013).
37. Uhlen, M. et al. Proteomics. Tissue-based map of the human proteome. *Science* **347**, 1260419 (2015).
38. Wishart, D. S. et al. DrugBank: a comprehensive resource for in silico drug discovery and exploration. *Nucleic Acids Res.* **34**, D668–D672 (2006).
39. Becher, I. et al. Thermal profiling reveals phenylalanine hydroxylase as an off-target of panobinostat. *Nat. Chem. Biol.* **12**, 908–910 (2016).
40. Wilhelm, M. et al. Mass-spectrometry-based draft of the human proteome. *Nature* **509**, 582–587 (2014).

Methods

Experimental design. In our study we aimed to create a comprehensive atlas of protein melting behavior derived from organisms living in different environmental niches and temperature conditions. For this purpose, we melted proteomes of different organisms starting from their OGT and extending this up to 30 °C above OGT. For some species (*O. antarctica*, *Arabidopsis thaliana*, *C. elegans*, *Saccharomyces cerevisiae* and *D. rerio*) for which we did not observe melting behavior beyond 10 °C above OGT, we adjusted the melting range as specified in Supplementary Table 1 to cover the whole melting range of the organism. All temperature points were encoded with TMT-10 reagents and measured on LC–MS/MS. The TMT ion intensity was then used for curve fitting along the melting gradient (see next for details). Detailed information on experimental design and reagents are collected in the Life Sciences Reporting Summary published alongside the presented work.

Organism growth and lysis conditions. Conditions for cell and organism growth and lysis are summarized in Supplementary Table 1. Briefly, all microorganisms (*O. antarctica* RB-8, *B. subtilis* 168, *E. coli* K12 MG1655, *Geobacillus stearothermophilus* NCA 26, *P. torridus* DSM 9790, *T. thermophilus* HB27) were obtained from the DSMZ (German Collection of Microorganisms and Cell Cultures) and cultured according to their recommendations. *P. torridus* medium was adjusted to pH 0.7 using sulfuric acid. Full medium for *T. thermophilus* HB27 was prepared using Aqua Purania water (TSI). *B. subtilis*, *E. coli*, *G. stearothermophilus* and *T. thermophilus* were grown overnight in 250 ml of full medium while shaking at 180 r.p.m. *P. torridus* was cultured in 100 ml of medium for 2 d, shaking at 50 r.p.m. *O. antarctica* culture (2L) was harvested 7 d after inoculation (15 °C, 120 r.p.m.). After cultivation, bacterial cultures were washed twice with ice-cold PBS. *P. torridus* was the only exception being washed with 50 mM sodium acetate (pH 4.6) to prevent cell lysis. For lysis, bacterial cell pellets were resolubilized in ice-cold PBS containing 0.5% Nonidet P-40 (Sigma) and protease inhibitors, and sonicated on ice for 15–20 min (frequency 0.5 s, amplitude 30%) using an ultrasonic processor UP200S (Hielscher Ultrasonics). *B. subtilis* was additionally passaged three times through a french pressure cell press (American Instruments Company Inc.). Bacterial cell lysates were then centrifuged for at least 30 min (21,000 relative centrifugal force (rcf), 4 °C).

Seedlings of *A. thaliana* ecotype Columbia-0 (Col-0) were grown for 7 d under continuous light conditions at 22 °C on Murashige and Skoog (½ MS) plates. Frozen plant material was homogenized with a Tissuelyzer (Qiagen) and stored at −80 °C. Mouse liver tissues were frozen in liquid nitrogen and disrupted into powder before lysis. Subsequently, the tissue was lysed in ice-cold PBS with 0.5% NP-40 and protease inhibitors by four cycles of snap-freezing in liquid nitrogen and cleared by centrifugation for 20 min at 20,000 rcf and 4 °C.

Mixed populations of *C. elegans* wildtype N2 (var. Bristol) were grown for 5 d at 20 °C on nematode growth medium agar plates with *E. coli* OP50 as food source. The nematodes were washed five times with M9 buffer before lysis. After the primary bead-beating procedure, worms were lysed in PBS containing 0.5% NP-40 and protease inhibitors.

Zebrafish endothelial (Zendo) cells[41] were cultured in Leibovitz L15 glutamax medium (Gibco) complemented with 14% fetal calf serum, 7.5 mM calcium chloride, 50 U ml^{-1} penicillin, 0.05 mg ml^{-1} streptomycin and 10 mg ml^{-1} gentamycin. They were cultured at 27 °C without CO_2 supply. Before collection, cells were washed twice in ice-cold PBS, followed by mechanical detachment. Cells were centrifuged for 5 min at 1,200 r.p.m., resuspended in PBS containing protease inhibitors and lysed by five freeze–thaw cycles. The lysate was cleared by centrifugation for 10 min at 20,000 rcf and 4 °C.

S. cerevisiae strain BY4741 (EuroSCARF) was cultured to the exponential growth phase at 30 °C in synthetic defined medium. The synthetic defined medium contained per liter: 6.7 g of yeast nitrogen base (Difco, B/C Biosciences), 20 g of glucose, 20 mg of adenine, 20 mg of arginine, 20 mg of histidine, 60 mg of leucine, 230 mg of lysine, 20 mg of methionine, 300 mg of threonine, 20 mg of tryptophan and 20 mg of uracil. The cells were collected by centrifugation at 3,000 rcf for 4 min, washed with MilliQ and stored at −20 °C until further processing. Pellet corresponding to 50 optical density (OD) was resuspended in 600 µl of ice-cold PBS containing protease inhibitors. In addition, 500 µl of 425–600 nm acid-washed glass beads (Sigma) was added. *S. cerevisiae* was lysed by bead beating for ten cycles (30 s on/30 s off). The lysate was cleared by centrifugation for 10 min at 20,000 rcf and 4 °C.

Drosophila melanogaster SII cells were cultured at 28 °C in complete Schneider's *Drosophila* medium containing 10% FBS and washed with PBS before lysis. Cells were lysed with PBS containing 0.5% NP-40 and protease inhibitors by four snap-freezing cycles in liquid nitrogen and the lysates were cleared by centrifugation for 20 min at 20,000 rcf and 4 °C.

Human cell lines were grown in recommended culture media. For thermal profiling of proteins in lysates, cells were washed in PBS and lysed either in PBS or PBS containing 0.5% NP-40 by four snap-freezing cycles in liquid nitrogen, and cleared by centrifugation for 20 min at 20,000 rcf and 4 °C. For thermal profiling of proteins in intact cells, cultures were washed in PBS, heated to the designated temperatures, lysed either in PBS or PBS containing 0.5% NP-40 by four snap-freezing cycles in liquid nitrogen and cleared by centrifugation for 20 min at 100,000 rcf and 4 °C.

Thermal profiling and protein digestion. TPP was performed as previously described[2]. Briefly, protein concentrations were determined by the Bradford Assay (Coomassie Protein Assay Kit, Thermo Fisher Scientific).

Lysates from all microorganisms, *A. thaliana*, *C. elegans*, *D. melanogaster* and mouse liver tissue were adjusted to 2 mg of protein per ml, divided into 100-µl aliquots and heated up in a PCR cycler (Flex Cycler 2, Biometra) at different temperatures for 3 min, then cooled to 25 °C for 5 min and placed on ice. Samples were ultracentrifuged at 100,000 rcf for 20 min at 4 °C. The protein concentration of the supernatants was estimated as above (Coomasie Protein Assay Reagent, Thermo Fisher Scientific) and stored at −80 °C until further analysis. For all in-gel digested samples, volumes corresponding to 50 µg of protein in the lowest temperature point were subjected to reduction (10 mM DTT, 45 min, 37 °C) and alkylation (55 mM chloroacetamide, 30 min, room temperature, in the dark). Samples were mixed with NuPAGE LDS sample buffer, denatured for 5 min at 96 °C and allowed to run 1 cm into a LDS–PAGE gel, leaving single bands, which were then cut out and placed in a drilled 96-well plate. Remaining solvent was removed by centrifugation at 1,000 r.p.m. for 1 min. The gel was destained with 100 µl of 50 mM TEAB in 50% ethanol for 2 h at room temperature and subsequently for 1 h at 50 °C. Gel pieces were dehydrated by adding 100% ethanol for 10 min at room temperature and washed with 100 µl of 5 mM TEAB for 20 min at room temperature. For digestion, 20 µl of 10 ng $µl^{-1}$ trypsin in 5 mM TEAB was added and incubated for 15 min at 4 °C. Remaining trypsin was removed by centrifugation and the digestion was performed overnight at 37 °C by adding 20 µl of 5 mM TEAB. The next day, peptides were acidified with 5 µl of 5% formic acid (FA) and extracted in three steps. In the first and second extraction, 20 µl of 1% FA were added and incubated for 30 min at room temperature. In the last extraction step 20 µl of 60% acetonitrile (ACN) in 0.1% FA were added and incubated for 30 min at room temperature. Eluted peptides were dried twice with 30 and 20 µl ACN for 15 min at room temperature and stored at −20 °C until further processing.

Protein concentration in *D. rerio* and *S. cerevisiae* lysates was determined by the BCA protein assay kit (Thermo Fisher Scientific), adjusted to 2 mg ml^{-1} and divided in ten 100 µl aliquots. Heat treatment was performed in a PCR cycler (T100 thermal cycler, Bio Rad) for 3 min, cooled down to 25 °C for 3 min and afterward placed on ice. For Zendo cells, a temperature range from 34 to 63.7 °C was chosen, for *S. cerevisiae*, a temperature range of 37 to 64 °C was chosen. Precipitate was removed by ultracentrifugation at 100,000 rcf for 1 h at 4 °C. Volume corresponding to 100 µg of protein at the lowest temperature point was taken. Samples were reduced and alkylated for 15 min in the dark at 37 °C (6 M urea, 10 mM TCEP and 40 mM CAA in 50 mM TEAB (pH 8.5)). Samples were further diluted with 3 volumes of 50 mM TEAB and trypsin was added (1:100 protease:protein ratio). Predigestion was performed for 2 h at 37 °C. A second overnight digestion step was performed by adding trypsin (1:100 protease:protein ratio). Digestion was stopped by acidifying to pH 2 by adding FA. Samples were centrifuged at 20,000 rcf for 10 min at 4 °C before they were desalted using 1-cm^3 Sep-Pek SPE cartridges (Waters). Briefly, cartridges were washed three times with 1 ml of ACN followed by washing three times with 1 ml of 0.1 M acetic acid. Samples were loaded and the flow-through was passed through the cartridges again. Cartridges were washed three times with 1 ml of 0.1 M acetic acid and the peptides were eluted using three times 250 µl of 0.1 M acetic acid/80% ACN. Samples were dried in a Thermo Savant SPD SpeedVac (Thermo Fisher Scientific).

TMT stable isotope labeling. TMT labeling for all in-gel digested samples was conducted as previously described and the TMT-126 channel was used for the lowest temperature in each experiment[42]. Briefly, protein digests were dissolved in 16 µl of 50 mM HEPES (pH 8.5) and mixed for 10 min at 20 °C. TMT reagent, dissolved in 100% anhydrous ACN, was added to each vial to a final concentration of 10.7 mM. Samples were incubated with shaking at 400 r.p.m. on a thermomixer for 1 h at 20 °C. The reaction was stopped by adding hydroxylamine to final concentration of 0.4% and incubating for 15 min at 20 °C and 400 r.p.m. on the thermoshaker. After TMT labeling, samples were combined and acidified using 20 µl of 10% FA. Samples were desalted on 50-mg Sep-Pak tC18 solid-phase extraction cartridges (Waters; wash solvent, 0.1% FA; elution solvent, 60% ACN in 0.1% FA).

Protein digests from *D. rerio* and *S. cerevisiae* were dissolved in 40 µl of 50 mM HEPES (pH 8.5) and mixed for 10 min at 20 °C. TMT reagents were dissolved in 42 µl of 100% anhydrous ACN, after which 10 µl of this solution was added to the peptides. Labeling was performed for 1 h at 20 °C while shaking at 400 r.p.m. The reaction was stopped by adding hydroxylamine to a final concentration of 0.4% and incubating for 15 min at 20 °C and 400 r.p.m. Subsequently, samples were pooled and acidified to pH 2 using FA. Samples were desalted using 1-cm^3 Sep-Pak SPE cartridges as described before. After desalting samples were dried using SpeedVac.

Peptide fractionation before LC–MS/MS analysis. All sample pools except for human, *D. rerio* and *S. cerevisiae* were fractionated on a Trinity P1 column (Thermo Fisher Scientific) using a Dionex Ultimate 3000 high-performance

liquid chromatography (HPLC) System (Dionex Corporation) as previously described[43]. Samples (100 µg) were loaded onto the column in Trinity solvent A (10 mM ammonium acetate in water, pH 4.7) and separated using 45 min gradient of 0–100% Trinity solvent B (10 mM ammonium acetate in 95% ACN, pH 5.4) at a flow rate of 250 µl min^{-1}. During separation, 32 fractions (1 min each) were collected. Samples from microorganisms were pooled into eight fractions and dried down in a SpeedVac, whereas samples from eukaryotic species were dried down without pooling. All human samples were fractionated via hydrophilic strong anion exchange (hSAX) chromatography as previously described[44,45]. Briefly, an equivalent of 200 µg protein digest was reconstituted in hSAX solvent A (5 mM Tris-HCl, pH 8.5) and separated using a Dionex Ultimate 3000 HPLC System (Dionex) equipped with an IonPac AG24 guard column (2 × 50 mm^2) and an IonPac AS24 strong anion exchange column (2 × 250 mm^2, Thermo Fisher). Samples were loaded onto the column and washed at a flow rate of 250 µl min^{-1} using 100% hSAX solvent A for 2 min and subsequently separated by increasing hSAX solvent B (5 mM Tris-HCl, pH 8.5, 1 M NaCl) from 3–27% in 24 min and to 40% in 13 min. After washing the column for 10 min at 100% hSAX solvent B, it was equilibrated with 100% hSAX solvent A. During separation, 40 fractions (1 min each) were collected. Afterward, fractions were acidified with 5 µl of neat FA and less-complex early and late fractions were pooled with more complex fractions eluting in the middle of the gradient. The resulting 24 fractions were desalted using self-packed StageTips (three disks, diameter 1.5 mm, C18 material, 3 M Empore; wash solvent, 0.1% FA; elution solvent, 0.1% FA in 50% ACN). Eluted fractions were frozen, dried down in a SpeedVac and stored at −20 °C until LC–MS analysis.

Sample pools from *D. rerio* and *S. cerevisiae* were fractionated using high pH reverse-phase HPLC fractionation using a Kinetex 5u EVO C18 100 A column (Phenomenex) on a HPLC 1200 system (Agilent) operating at a flow rate of 200 µl min^{-1}. Briefly, dried pellet was reconstituted in 20 µl of buffer A (10 mM NH_4OH, pH 10) and injected. Samples were first loaded on the column at a flow rate of 20 µl min^{-1} for 2 min. Peptides were eluted stepwise using the following gradient: 2–12% buffer B (10 mM NH_4OH/90% ACN, pH 10) in 6 min, 12–35% buffer B in 47 min, 35–55% buffer B in 7 min, 55–100% buffer B in 3 min, 0–100% buffer A in 9 min and 100% buffer A for 31 min. A total gradient time of 105 min was used. Fractions corresponding to 1 min of gradient time were collected on a 1260 infinity fraction collector (Agilent). Only fractions eluting after 8 min were collected. These fractions were concatenated in 15 fractions for Zendo cells and ten fractions for *S. cerevisiae*. All the fractions were dried down using SpeedVac and stored at −80 °C until further use.

TPP of drugs. For the two-dimensional TPP of tranylcypromine (TCP) (Selleckchem) in lysate, THP1 cells were washed twice using PBS, resuspended in ice-cold PBS supplemented with protease inhibitor and snap-frozen in liquid nitrogen. Following five freeze–thaw cycles, cells were Dounce homogenized with 20 strokes and centrifuged at 100,000 rcf (20 min, 4 °C). Protein concentration was determined by Bradford assay. The lysate was adjusted to 2 mg of protein per ml and 100 µl of THP1 cell lysate per condition (ten concentrations at five temperatures) were incubated for 20 min at 25 °C with either vehicle (ddH_2O) or tranylcypromine (0.1, 0.3, 1, 3, 10, 30, 100, 300 and 1,000 µM) before samples were heated for 3 min to the target temperatures (44, 48, 52, 56 or 60 °C). After incubation for 3 min at room temperature and 6 min on ice, aggregated proteins were pelleted at 100,000 rcf (20 min, 4 °C).

For the melting curve based TPP of the dihydrofolate reductase inhibitor trimethoprim (Sigma-Aldrich) *E. coli* cells were washed twice with PBS supplemented with 0.4% NP-40 and lysed by sonication. Protein concentration was determined via Bradford assay, and the bacterial cell extract was distributed into aliquots with a final protein concentration of 2 mg ml^{-1}. The cell extract was incubated with 25 µM trimethoprim or vehicle (DMSO) for 30 min at room temperature and heated to the target temperatures (37.0, 39.9, 43.0, 46.6, 50.2, 53.8, 57.4, 61.0, 64.1 or 67.0 °C) for 3 min and cooled down on ice for 10 min previous ultracentrifugation (>100,000*g*, 20 min, 4 °C) to pellet aggregated proteins.

For subsequent protein digestion, 80 µl of the supernatants were dried down and resuspended in 6 M urea in 40 mM Tris-HCl (pH 7.6). After reduction (10 mM DTT, 30 °C, 30 min) and alkylation (50 mM chloroacetamide, room temperature, 30 min, in the dark), samples were diluted to 1.2 M urea using 40 mM Tris-HCl (pH 7.6) and digestion was performed overnight at 37 °C and 500 r.p.m. using trypsin (Promega, 1:50 enzyme:substrate ratio). Digests were acidified by addition of neat FA to 1% and desalted using a Sep-Pak C18 96-well plate (Waters) (wash solvent, 0.1% FA; elution solvent, 0.1% FA in 50% ACN). TMT labeling was conducted as described before, combining samples treated with increasing TCP concentrations and heated to the same temperature in one TMT-10plex experiment. High pH reversed phase tip fractionation was performed as previously described[42]. Briefly, an aliquot of each sample pool corresponding to 40 µg of initial protein input was resuspended in 0.1% FA, and desalted (wash solvent, 0.1% FA; elution solvent, 0.1% FA in 50% ACN) and fractionated (wash solvent, 25 mM NH_4COOH, pH 10; elution solvents, 25 mM NH_4COOH (pH 10) in 7.5, 10, 12.5, 15, 20, 25 and 50% ACN) using self-packed StageTips (five disks, diameter 1.5 mm, C18 material, 3 M Empore). The sample flow-through was combined with the 25% ACN eluate and the 7.5% ACN with the 50% ACN fraction, resulting in a total of six fractions that were dried down and stored at −20 °C until LC–MS measurement.

LC–MS/MS analysis. Here, 1 µg of each Trinity or hSAX fraction was resuspended in 0.1% FA in water and injected into an Ultimate 3000 RSLCnano System (Thermo Fisher Scientific) coupled to a Q-Exactive Plus or Fusion Lumos Tribrid mass spectrometer (Thermo Fisher Scientific; see Supplementary Table 1 for details). Peptides were delivered to a trap column (75 µm × 2 cm, packed in house with 5 µm C18 resin, Reprosil PUR AQ, Dr Maisch), washed for 10 min at a flow rate of 5 µl min^{-1} in loading solvent (0.1% FA in water) and separated on the analytical column (75 µm × 45 cm, packed in house with 3 µm C18 resin, Reprosil Gold, Dr Maisch) applying a flow rate of 300 nl min^{-1} and using a 90 min gradient of 2–80% solvent B (LC solvent A, 0.1% FA, 5% DMSO; LC solvent B, 0.1% FA, 5% DMSO in ACN). DMSO as solvent additive was used to boost the nESI signal of peptides[46]. The Q-Exactive Plus was operated in data-dependent acquisition and positive ionization mode. Full-scan MS1 spectra were acquired from 360 to 1,300 *m/z*, at 60,000 resolution, using an automatic gain control (AGC) target value of 3×10^6 (Q-Exactive) or 4×10^5 (Lumos) charges and a maximum injection time (maxIT) of 10 ms. Up to 25 precursor ions were allowed to be selected for fragmentation. Dynamic exclusion was set up to 25 s. MS2 spectra were acquired at 30,000 resolution with a fixed first mass of 100 *m/z* and using an AGC target value of 2×10^5 charges and a maxIT of 50 ms.

For the meltome analysis of *D. rerio* and *S. cerevisiae*, 1 µg of peptide was dissolved in 10% FA and injected on an ultra-HPLC 1290 system (Agilent) coupled to a Q-Exactive HF-X mass spectrometer (Thermo Fisher scientific). Peptides were trapped (Dr Maisch Reprosil C18, 3 µm, 2 cm × 100 µm) before being separated using an analytical column (Agilent Poroshell EC-C18, 2.7 µm, 50 cm × 75 µm). Trapping was performed for 5 min in buffer A (0.1% FA) at a flow rate of 0.005 ml min^{-1}. The following gradient was used for separation: 12–42% buffer B (80% ACN + 0.1% FA) in 95 min, 100% buffer B for 2 min followed by 100% buffer A for 11 min. The flow was split to generate a final flow of 300 nl min^{-1}. The Q-Exactive HF-X was operated in a data-dependent acquisition mode with positive ionization. Full MS spectra were acquired from 375–1,500 *m/z* at 60,000 resolution, using an AGC target value of 3×10^6 charges and a maximum injection time of 20 ms. A maximum of 12 precursors were allowed to be fragmented. A dynamic exclusion of 18 s was used. MS2 fragmentation spectra were obtained with a fixed first mass of 120 *m/z* at 45,000 resolution, using an AGC target of 1×10^5 and a maximum injection time of 85 ms. Fragmentation was performed using higher-energy collisional dissociation (HCD) at a normalized collision energy (NCE) of 32.

MS measurements for samples from the two-dimensional proteome profiling using TCP were performed on a Fusion Lumos Tribrid mass spectrometer (Thermo Fisher Scientific) as described above with following modifications: a 100-min linear gradient from 6 to 34% LC solvent B in LC solvent A was applied. Full-scan MS1 spectra were obtained using an AGC target value of 4×10^5 charges and a maxIT of 20 ms. MS2 spectra for peptide identification were obtained in the ion trap in rapid scan mode via sequential isolation of up to ten precursors (isolation window 0.7 *m/z*, AGC target value of 2×10^4, maxIT of 100 ms, dynamic exclusion of 90 s) and fragmentation via CID (NCE of 35%, activation Q of 0.25). For TMT reporter quantification, each peptide precursor was fragmented again, followed by the synchronous selection of up to ten of most intense peptide fragments in the ion trap and further fragmentation via HCD using a NCE of 55%. MS3 spectra were recorded in the orbitrap at 50,000 resolution (scan range 100–1,000 *m/z*, charge dependent isolation window from 1.3 (2+) to 0.7 (5–6+) *m/z*, AGC of 1.2×10^5 charges, maxIT of 120 ms).

LC–MS/MS measurements of *E. coli* samples of the trimethoprim experiment were performed on an Ultimate 3000 RSLCnano System coupled to the Q-Exactive Plus instrument as described before.

Peptide and protein identification by database searching. Peptide and protein identification and quantification were performed using MaxQuant (v.1.5.5.1) with its embedded Andromeda search engine. Spectra were searched against the SwissProt canonical databases downloaded for all analyzed organisms and supplemented with common contaminants. Trypsin/P was selected as proteolytic enzyme and up to two missed cleavage sites were allowed. Carbamidomethylation of cysteine was set as fixed modification, and oxidation of methionine and N-terminal protein acetylation as variable modifications. TMT10 was specified as label within a reporter ion MS2 (meltome data) or MS3 (two-dimensional thermal profiling data) experiment type. The mass tolerance of precursor ions was set to ±5 ppm and of fragment ions to ±20 ppm for orbitrap and 0.5 Da for ion trap spectra. Results were adjusted to 1% peptide spectrum match and 1% protein false discovery rate employing a target-decoy approach using reversed protein sequences.

Inference of protein melting points. Protein melting points were determined by fitting sigmoidal curves to relative protein abundances using the TPP 'R' package as described previously[2]. First, relative abundances were obtained by normalizing absolute TMT reporter intensities with the reporter intensity corresponding to the

lowest temperature channel. Then, melting curves with three free parameters *a*, *b* and plateau of the form

$$f(T) = \frac{1 - \text{plateau}}{1 + e^{-\left(\frac{a}{T} - b\right)}} + \text{plateau}$$

were fitted numerically to the relative abundances as a function of temperature *T*. In this model, $f(T)$ is by definition fixed to one at the lowest temperature. The T_m is defined as the temperature at which the inferred melting curve first hits a relative protein abundance of 50% compared to the lowest temperature data point (defined as 100%); that is, $f(T_m) = 0.5$. To allow comparisons between proteins without defined T_m, such as nonmelters, protein melting behavior was additionally quantified using the AUC. The AUC was computed by numerical integration of the melting curve between the lowest and highest measured temperature points for the respective species. All proteins with assigned T_m were characterized as melters and the remaining proteins without T_m values we classified as nonmelters. All melters with AUC < 0.35 were called low-T_m melters, those with AUC > 0.65 were named high-T_m melters and the remaining melting proteins were called medium-T_m melters.

Computation of absolute protein abundance. Absolute protein abundance was estimated from adjusted MS1 intensities as described previously[31]. Briefly, first, the relative contribution of the lowest temperature channel to the overall MS1 intensity (which contains all isobaric TMT channels) was estimated as the fraction of its TMT reporter intensity among the sum of all MS2 reporter intensities. The MS1 intensity of the protein was then multiplied by this fraction, and divided by the number of theoretically observable peptides to obtain the iBAQ (intensity-based absolute quantification) as described previously[47].

Functional enrichment analyses. Gene ontology and UniProt sequence feature annotations for functional enrichment/depletion analyses were obtained from DAVID[48] and tested for significant differences between groups using the Fisher Exact test. *P* values were corrected for multiple testing using the Benjamini–Hochberg procedure (see also the Statistical analysis section).

Prediction of protein structural features from sequence. For the comparison of melting points to structural features of the protein, secondary structure and disordered residues were predicted from protein primary sequence using PredictProtein[49]. For quantitative and categorical comparisons of structural features to protein stability, the absolute number of residues predicted with a certain secondary structure (helix, strand, coil) or disorder assignment (disordered, not disordered) was normalized by overall protein length. The tabular data underlying the plots presented in the manuscript can be found at proteomeXchange (data set identifier PXD011929).

Melting point comparisons between different species. Melting points of orthologous proteins were compared between different species based on the KEGG Orthology database[50] obtained via UniProt. For all orthologs of each pair of species, the Pearson and Spearman correlation coefficients of the AUCs of protein melting curves were estimated. To correct the correlation coefficients for spurious correlations arising from bias in the AUC distributions such as bimodality, the correlation coefficient for each species pair was corrected by randomly shuffling the data and computing a correlation coefficient 10,000 times and then subtracting the 99th percentile of this random background distribution from the correlation coefficient computed on the actual data.

Construction of genomic libraries of *T. thermophilus* for expression in *E. coli*. Genomic DNA of *T. thermophilus* HB27 was isolated with the MasterPure DNA Purification Kit (Epicentre) from overnight cultures and fragmented with a Hamilton Microliter no. 710 syringe (Hamilton Bonaduz) into fragments of roughly 40 kilobasepairs in length. These fragments were then used as inserts to construct a pCC1FOS fosmid library in EPI300 T1^R cells using the CopyControl Fosmid Library Production Kit (Epicentre). From these libraries, 288 clones carrying fragments of the *T. thermophilus* genome (estimated genome coverage of 4.6-fold) were selected and cultivated in deep-well plates (1 ml of LB medium + 12.5 μg ml^{-1} chloramphenicol per well, 37 °C, 150 r.p.m.). After 2 d of cultivation, the cells were pooled and washed twice in ice-cold PBS with centrifugation steps in-between (4,500 r.p.m., 4 °C). Cells were stored as pellets at −20 °C.

Oxygen consumption in intact and permeabilized HEK293 cells. Respiration of HEK293 cells was measured in a high-resolution respirometer (OROBOROS Oxygraph-2k) containing two individual glass chambers. Oxygen concentration was automatically calculated by the DatLab software (v.7.0.0.2) depending on barometric pressure and the solubility factor of the buffer. Oxygen calibration at air saturation was performed every day. Data were recorded using DatLab. For respiration measurements, intact HEK293 cells or HEK293 cells that were permeabilized with the detergent α-tomatine for accessing the activity of the different respiratory chain complexes were used. Cells were suspended in mitochondrial respiration medium (Mir05) and prepared according to the manufacturer's instructions (Gnaiger E 2000). Intact and permeabilized cells were applied into separate glass chambers together with the different substrates, uncouplers and inhibitors. Intact HEK293 cells were left for some minutes until respiration was stable. Glucose (5 mM) was applied to activate glycolysis and mitochondrial respiration. After oxygen consumption reached a stable level again, the protonophore carbonyl cyanide-p-trifluoromethoxyphenylhydrazone (FCCP) was titrated in 0.5-μM steps until maximal respiratory capacity was reached. Subsequently, the complex III inhibitor Antimycin A (1 μg ml^{-1}) was added to inhibit the respiratory chain and obtain nonmitochondrial respiration, which was subtracted from the different respiratory values during data evaluation. Permeabilized cells were treated with substrates for complex I and II (5 mM pyruvate, 2 mM malate, 5 mM succinate) to induce leak respiration of the cells. After oxygen consumption levels reached a stable plateau, 5 mM ADP were applied evoking maximal coupled respiration. Concomitantly, the protonophore FCCP was titrated in 0.5 μM steps until the maximal respiratory capacity was reached. The application of antimycin A (1 μg ml^{-1}) resulted in nonmitochondrial respiration, which was subtracted from the different respiratory values during data processing.

Statistical analysis. Unless otherwise noted, data are presented as mean ± s.d. Statistical significance was calculated by standard unpaired one- or two-way analysis of variance (ANOVA) with Bonferroni posttest correction, by nonparametric two-sided Wilcoxon–Mann–Whitney or by the Kruskal–Wallis and Dunn's post hoc tests. Multiple testing corrections were carried out using the Benjamini–Hochberg or Bonferroni procedures. $P < 0.05$ was considered statistically significant. Further details regarding statistical analysis are described below the respective figures.

Reproducibility analysis. The reproducibility of TPP experiments was assessed at three levels and the results are summarized in Supplementary Fig. 2.

(1) Reproducibility of LC–MS/MS analysis. TMT-labeled digests of *S. cerevisiae* and *D. rerio* were split into three aliquots and each was measured by nanoLC–MS/MS on a Q-Exactive HF-X mass spectrometer in the Utrecht laboratory. The replicates R1, R2 and R3 for these species represent identical samples.
(2) Reproducibility of the TPP workflow. The European Molecular Biology Laboratory (EMBL) and OmicScouts (OS) laboratories performed at least two independent workflow replicates of the human samples and these were measured on the same nanoLC–MS/MS instrument. The replicates R1, R2, …, Rn for the human samples represent TPP workflow replicates. The Technical University of Munic (TUM) laboratory performed two independent workflow replicates of all microorganisms (*E. coli*, *E. coli* on cells experiment, *E. coli* Arctic Express, *T. thermophilus*, *T. thermophilus* on cells experiment, *O. antarctica*, *B. subtilis*, *G. stearothermophilus*, *P. torridus*) and further eukaryotic species (*A. thaliana*, *C. elegans*, *D. melanogaster*, *M. musculus* liver tissue). The two workflow replicates R1 and R2 were measured on the same microLC–MS/MS instrument. In addition, workflow replicate R1 was also measured on a nanoLC–MS/MS instrument (denoted R3).
(3) Inter-laboratory reproducibility. Aliquots of the same batch of human K562 cells were distributed across the TUM, EMBL and OS laboratories. Two independent workflow replicates using the same conditions for thermal profiling (on cells) were performed in each laboratory. Equipment and conditions for sample digestion, TMT labeling, prefractionation and LC–MS/MS analysis were performed according to the respective internal laboratory protocols.

Reporting Summary. Further information on research design is available in the Nature Research Reporting Summary linked to this article.

Data availability

Supplementary Information is available in the online version of this manuscript. The mass spectrometry raw files, peptide and protein identification search engine output files and files showing the melting curves for all proteins have been deposited with the proteomeXchange consortium via the PRIDE partner repository under the project name 'Meltome atlas—thermal proteome stability across the tree of life' and the data set identifier PXD011929.
The melting curves for all proteins are also available in the online R Shiny App http://meltomeatlas.proteomics.wzw.tum.de:5003/. The human meltome data are also available at https://www.proteomicsdb.org. Files containing data sources for main text figures can be downloaded from https://figshare.com/account/home#/projects/75567. Source data for Figs. 2–6 are presented with the paper.

Code availability

Code for data analysis is available for download at Bioconductor: https://bioconductor.org/packages/release/bioc/html/TPP.html.

References

41. Choorapoikayil, S., Overvoorde, J. & den Hertog, J. Deriving cell lines from zebrafish embryos and tumors. *Zebrafish* **10**, 316–325 (2013).

42. Ruprecht, B., Zecha, J., Zolg, D. P. & Kuster, B. High pH reversed-phase micro-columns for simple, sensitive, and efficient fractionation of proteome and (TMT labeled) phosphoproteome digests. *Methods Mol. Biol.* **1550**, 83–98 (2017).
43. Yu, P. et al. Trimodal mixed mode chromatography that enables efficient offline two-dimensional peptide fractionation for proteome analysis. *Anal. Chem.* **89**, 8884–8891 (2017).
44. Ruprecht, B. et al. Hydrophilic strong anion exchange (hSAX) chromatography enables deep fractionation of tissue proteomes. *Methods Mol. Biol.* **1550**, 69–82 (2017).
45. Ruprecht, B. et al. in *Proteomics: Methods and Protocols* (eds Comai, L. et al.) 69–82 (Springer, 2017).
46. Hahne, H. et al. DMSO enhances electrospray response, boosting sensitivity of proteomic experiments. *Nat. Methods* **10**, 989–991 (2013).
47. Schwanhausser, B. et al. Global quantification of mammalian gene expression control. *Nature* **473**, 337–342 (2011).
48. Huang da, W., Sherman, B. T. & Lempicki, R. A. Systematic and integrative analysis of large gene lists using DAVID bioinformatics resources. *Nat. Protoc.* **4**, 44–57 (2009).
49. Yachdav, G. et al. PredictProtein-an open resource for online prediction of protein structural and functional features. *Nucleic Acids Res.* **42**, 337–343 (2014).
50. Kanehisa, M., Sato, Y. & Morishima, K. BlastKOALA and GhostKOALA: KEGG tools for functional characterization of genome and metagenome sequences. *J. Mol. Biol.* **428**, 726–731 (2016).

Acknowledgements

The data reported here are tabulated in the main paper and Supplementary Information. We thank P. Giansanti for providing the mouse samples; A. Hubauer and S. Petzoldt for technical assistance; M. Übelacker for assistance with bacterial cultivation; I. Cornella-Taracido (Merck Research Laboratories, Boston, MA), C. Siegl, S. Dieter and H. Glimm (NCT Heidelberg, Germany); A. Augustin (Hoffmann-La Roche, Basel, Switzerland) and colleagues for providing access to their meltome data; and M. Bernhofer, J. Reeb and B. Rost for computing and providing protein structure predictions. A.J. is grateful for funding from the Alexander von Humboldt foundation, J.Z. for funding from the German Consortium for Translational Cancer Research, P.S. for funding from SAP, J.M. for funding from the German Science Foundation (DFG-SFB924) and M.W. for funding from the ProteomeTools project (BMBF grant no. 031L0008A).

Author contributions

A.J. planned and performed experiments, contributed to data analysis, interpretation and manuscript writing. N.K. contributed to data analysis, interpretation and manuscript writing, wrote the shiny app. T.H. contributed to data analysis, interpretation and manuscript writing. M. Moerch contributed to planning and performing experiments. J.Z. performed and analyzed experiments. N.L. performed experiments. Y.B. contributed to data acquisition. E.M. and M. Maschberger performed experiments. G.S. contributed to data acquisition. I.B. and C.D. performed experiments. P.S. contributed to building the data repository ProteomicsDB. J.M. performed experiments. B.S. performed experiments. A.A. contributed to data analysis and interpretation. T.W. performed experiments. M.B. contributed to data analysis and interpretation. M.W. contributed to building the data repository ProteomicsDB. M.K. contributed to data analysis and interpretation. S.L. contributed to data analysis and interpretation. W.L. contributed to data analysis and interpretation. H.H. conceived the idea, supervised the studies, contributed to data interpretation and manuscript writing. M.M.S. conceived the idea, supervised the studies and contributed to data interpretation and manuscript writing. B.K. conceived the idea, supervised the studies and contributed to data interpretation and manuscript writing.

Competing interests

H.H. is cofounder, shareholder and CEO of OmicScouts GmbH. M.W. and B.K. are cofounders and shareholders of OmicScouts GmbH and msAId GmbH. M.W. and B.K. have no operational role in either company. T.W. and M.B. are employees and shareholders of GlaxoSmithKline. M.M.S. is a shareholder of GlaxoSmithKline.

Additional information

Supplementary information is available for this paper at https://doi.org/10.1038/s41592-020-0801-4.

Correspondence and requests for materials should be addressed to H.H., M.M.S. or B.K.

Peer review information Editor recognition statement: Arunima Singh was the primary editor on this article and managed its editorial process and peer review in collaboration with the rest of the editorial team.

nature research

Corresponding author(s): DBPR NMETH-RS39116C

Last updated by author(s): Feb 10, 2020

Reporting Summary

Nature Research wishes to improve the reproducibility of the work that we publish. This form provides structure for consistency and transparency in reporting. For further information on Nature Research policies, see Authors & Referees and the Editorial Policy Checklist.

Statistics

For all statistical analyses, confirm that the following items are present in the figure legend, table legend, main text, or Methods section.

n/a	Confirmed
☐	☒ The exact sample size (*n*) for each experimental group/condition, given as a discrete number and unit of measurement
☐	☒ A statement on whether measurements were taken from distinct samples or whether the same sample was measured repeatedly
☐	☒ The statistical test(s) used AND whether they are one- or two-sided *Only common tests should be described solely by name; describe more complex techniques in the Methods section.*
☐	☒ A description of all covariates tested
☐	☒ A description of any assumptions or corrections, such as tests of normality and adjustment for multiple comparisons
☐	☒ A full description of the statistical parameters including central tendency (e.g. means) or other basic estimates (e.g. regression coefficient) AND variation (e.g. standard deviation) or associated estimates of uncertainty (e.g. confidence intervals)
☐	☒ For null hypothesis testing, the test statistic (e.g. *F*, *t*, *r*) with confidence intervals, effect sizes, degrees of freedom and *P* value noted *Give P values as exact values whenever suitable.*
☒	☐ For Bayesian analysis, information on the choice of priors and Markov chain Monte Carlo settings
☐	☒ For hierarchical and complex designs, identification of the appropriate level for tests and full reporting of outcomes
☐	☒ Estimates of effect sizes (e.g. Cohen's *d*, Pearson's *r*), indicating how they were calculated

Our web collection on statistics for biologists contains articles on many of the points above.

Software and code

Policy information about availability of computer code

Data collection	Data was measured on Q Exactive Plus or HF-X and Fusion Lumos Tribrid mass spectrometer (Thermo Fisher Scientific) and collected by Xcalibur software (Thermo Fisher Scientific). Raw mass spectrometry files were analyzed by MaxQuant (v1.5.5.1) with embedded Andromeda search engine.
Data analysis	Data was analyzed by TPP R package (v. 3.12.0) published previously by Franken et al., Nat. Protoc., 2015 (this information will be added to the final version of the manuscript). wBoot version 1.03 was used for the bootstrap test.

For manuscripts utilizing custom algorithms or software that are central to the research but not yet described in published literature, software must be made available to editors/reviewers. We strongly encourage code deposition in a community repository (e.g. GitHub). See the Nature Research guidelines for submitting code & software for further information.

Data

Policy information about availability of data

All manuscripts must include a data availability statement. This statement should provide the following information, where applicable:

- Accession codes, unique identifiers, or web links for publicly available datasets
- A list of figures that have associated raw data
- A description of any restrictions on data availability

Supplementary Information is available in an additional file. The mass spectrometry raw files, search engine output and thermal proteome profiling files have been deposited with the ProteomeXchange Consortium via the PRIDE partner repository (http://proteomecentral.proteomexchange.org) under the project name "Meltome" and the dataset identifier "PXD011929". All Meltome data can be explored online using shiny-app http://meltomeatlas.proteomics.wzw.tum.de:5003/. Human meltome data is also available at ProteomicsDB (https://www.proteomicsdb.org). Data sources for main figures can be downloaded at https://figshare.com/account/home#/projects/75567

Field-specific reporting

Please select the one below that is the best fit for your research. If you are not sure, read the appropriate sections before making your selection.

☒ Life sciences ☐ Behavioural & social sciences ☐ Ecological, evolutionary & environmental sciences

For a reference copy of the document with all sections, see nature.com/documents/nr-reporting-summary-flat.pdf

Life sciences study design

All studies must disclose on these points even when the disclosure is negative.

Sample size	Our studies present 77 data sets from 13 species including 6 prokaryotes (five bacteria and one archaeon) and 7 eukaryotes. Detalied analysis is performed on human samples, represented by 14 different cell lines and 5 body fluids. Most of the species chosen for Meltome analysis are model organisms, which are used through many biological studies and will serve as a repository for further studies.
Data exclusions	We have not excluded any data from our analysis.
Replication	We analysed all 77 data sets in at least two replicates and correlated either areas under the melting curve (AUC) or melting points (TM). Reproducibility analysis across replicates and laboratories was performed on the same batch of K562 cell line. Reproducibility within the same laboratory was better than between laboratories but the overall reproducibility was very good. 50% of all proteins had Tm and AUC values within 0.5°C and 3% respectively between replicates measured in the same laboratory. The variability was higher for replicates measured between laboratories but not worse than 2.3°C for Tm and 10% for AUC. (the above figures for 80% of all proteins are: TM of 1.5 °C and AUC of 8% for replicates measured in the same laboratory and TM of 4.5°C and AUC of 20% for replicates measured in different laboratories).
Randomization	No randomization was applied in our sample sets. For our Meltome atlas data set we have chosen the organisms, which are most frequently used in biological studies.
Blinding	Blinding was not relevant to our studies, since we present a resource data.

Reporting for specific materials, systems and methods

We require information from authors about some types of materials, experimental systems and methods used in many studies. Here, indicate whether each material, system or method listed is relevant to your study. If you are not sure if a list item applies to your research, read the appropriate section before selecting a response.

Materials & experimental systems

n/a	Involved in the study
☒	☐ Antibodies
☐	☒ Eukaryotic cell lines
☒	☐ Palaeontology
☒	☐ Animals and other organisms
☒	☐ Human research participants
☒	☐ Clinical data

Methods

n/a	Involved in the study
☒	☐ ChIP-seq
☒	☐ Flow cytometry
☒	☐ MRI-based neuroimaging

Eukaryotic cell lines

Policy information about cell lines

Cell line source(s)	Jurkat (ATCC), HaCaT (ATCC), K562 (ATCC and NCI), HepG2 (ATCC), HAOEC (ATCC), HL60 (ATCC), U937 (ATCC), HEK293T (ATCC), primary T cells (ATCC), A549 (ATCC), HEK293 (DSMZ-German Collection of Microorganisms and Cell Cultures), human lung fibroblasts (Lonza, Cat No. CC-2512; Donor Lot #430173), human plateable hepatocytes (Thermo Fisher Scientific, Cat No. HMCPP5)
Authentication	Jurkat, HaCaT, K562, HepG2, HAOEC, HL60, U937, HEK293T, A549, HEK293 were authenticated.
Mycoplasma contamination	All cell lines used in our studies were checked for mycoplasma and only mycoplasma-negative cell lines were used in further studies.
Commonly misidentified lines (See ICLAC register)	We have not used any of the commonly misidentified cell lines.